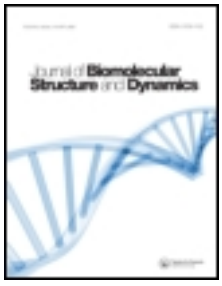

Journal of Biomolecular Structure and Dynamics
Publication details, including instructions for authors and subscription information:
http://www.tandfonline.com/loi/tbsd20

Molecular dynamics simulation to investigate the impact of disulfide bond formation on conformational stability of chicken cystatin I66Q mutant

Jianwei He [a], Linan Xu [a], Zhiyuan Zou [a], Nobuhiro Ueyama [b], Hui Li [a], Akio Kato [b], Gary W. Jones [c] & Youtao Song [a]

[a] Province Key Laboratory of Animal Resource and Epidemic Disease Prevention, Liaoning University, Shenyang, 110036, China

[b] Department of Biological Chemistry, Yamaguchi University, Yamaguchi, 753-8515, Japan

[c] National University of Ireland Maynooth, Maynooth, Co. Kildare, Ireland

Version of record first published: 02 Oct 2012.

To cite this article: Jianwei He , Linan Xu , Zhiyuan Zou , Nobuhiro Ueyama , Hui Li , Akio Kato , Gary W. Jones & Youtao Song (2012): Molecular dynamics simulation to investigate the impact of disulfide bond formation on conformational stability of chicken cystatin I66Q mutant, Journal of Biomolecular Structure and Dynamics, DOI:10.1080/07391102.2012.721498

To link to this article: http://dx.doi.org/10.1080/07391102.2012.721498

Journal of Biomolecular Structure and Dynamics
iFirst, 2012, 1–10

Molecular dynamics simulation to investigate the impact of disulfide bond formation on conformational stability of chicken cystatin I66Q mutant

Jianwei He[a], Linan Xu[a], Zhiyuan Zou[a], Nobuhiro Ueyama[b], Hui Li[a], Akio Kato[b], Gary W. Jones[c] and Youtao Song[a]*

[a]*Province Key Laboratory of Animal Resource and Epidemic Disease Prevention, Liaoning University, Shenyang 110036, China;* [b]*Department of Biological Chemistry, Yamaguchi University, Yamaguchi, 753-8515, Japan;* [c]*National University of Ireland Maynooth, Maynooth, Co. Kildare, Ireland*

Communicated by Ramaswamy H. Sarma

(*Received 19 June 2012; final version received 12 August 2012*)

Chicken cystatin (cC) mutant I66Q is located in the hydrophobic core of the protein and increases the propensity for amyloid formation. Here, we demonstrate that under physiological conditions, the replacement of Ile with the Gln in the I66Q mutant increases the susceptibility for the disulfide bond Cys71–Cys81 to be reduced when compared to the wild type (WT) cC. Molecular dynamics (MD) simulations under conditions favoring cC amyloid fibril formation are in agreement with the experimental results. MD simulations were also performed to investigate the impact of disrupting the Cys71–Cys81 disulfide bond on the conformational stability of cC at the atomic level, and highlighted major disruption to the cC appendant structure. Domain swapping and extensive unfolding has been proposed as one of the possible mechanisms initiating amyloid fibril formation by cystatin. Our *in silico* studies suggest that disulfide bond formation between residues Cys95 and Cys115 is necessary to maintain conformational stability of the I66Q mutant following breakage of the Cys71–Cys81 disulfide bridge. Subsequent breakage of disulfide bond Cys95–Cys115 resulted in large structural destabilization of the I66Q mutant, which increased the α–β interface distance and expanded the hydrophobic core. These experimental and computational studies provide molecular-level insight into the relationship between disulfide bond formation and progressive unfolding of amyloidogenic cC mutant I66Q.

An animated Interactive 3D Complement (I3DC) is available in Proteopedia at http://proteopedia.org/w/Journal:JBSD:23

Keywords: chicken cystatin; I66Q mutant; disulfide bond; molecular dynamics simulation.

Introduction

Human cystatin C (HCC) is an inhibitor of extracellular cysteine proteinases, and is found in all body fluids and tissues examined (Bobek & Levine, 1992). Human cystatin C amyloid angiopathy (HCCAA) is a dominantly inherited disorder characterized by tissue deposition of amyloid fibrils in blood vessels that leads to recurrent hemorrhagic stroke (Sanders et al., 2004). Wild type (WT) HCC forms a part of the amyloid deposits in brain arteries of elderly people with amyloid angiopathy (Olafsson & Grubb, 2000). The genetic background of a more severe HCCAA disease, which causes massive amyloidosis, cerebral hemorrhage, and death in young adults, is associated with a point mutation responsible for the amino acid substitution, a glutamine residue replacing a leucine residue at position 68 in the HCC polypeptide chain (Abrahamson, 1996). Recent studies showed that HCC associates with amyloid-β (Aβ) and can inhibit formation of Aβ fibrils and oligomers both *in vitro* and in mouse models of amyloid deposition, suggesting a possible role for HCC in Alzheimer's disease AD (Kaeser et al., 2007; Mi et al., 2007).

Chicken cystatin (Cc) is the most well-characterized member of the cystatin superfamily and displays similar biophysical characteristics with HCC, especially in terms of secondary structure and the amyloidogenic properties. The 3D structure of cC has been characterized by X-ray crystallography and nuclear magnetic resonance (NMR) (Bode et al., 1988; Engh et al., 1993). NMR studies confirmed that the 3D structure of cC is similar to that described for HCC (Ekiel et al., 1997). Residue 66 in cC, corresponding to residue 68 in HCC, lies buried in the hydrophobic core of the protein molecule. Research on cC

*Corresponding author. Email: ysong@lnu.edu.cn

ISSN 0739-1102 print/ISSN 1538-0254 online

http://dx.doi.org/10.1080/07391102.2012.721498
http://www.tandfonline.com

variant I66Q demonstrated that I66Q has similar amyloidogenic properties as HCC L68Q (He et al., 2005; Staniforth et al., 2001). The structures of both HCC and cC consist of a large five-stranded antiparallel β-sheet wrapped around a central α-helix, both structures possess two disulfide bonds. The connectivity within the β-strands is: (N)-β1-(α)-β2-L1-β3-(AS)-β4-L2-β5-(C), where AS is a broad 'appending structure' (Grubb et al., 1984). Both disulfide bonds of cC are located in the carboxy-terminal of the protein. The Cys71–Cys81 bond is contained in the AS and links a small segment of α-helical structure to the main β-sheet of the protein, the other disulfide bond, Cys95–Cys115, joins the two carboxy-terminal β-strands of the main β-sheet (Figure 1, Bode et al., 1988).

To date, 3D domain swapping has been observed in more than 30 different proteins (Ivanova, Sawaya, Gingery, Attinger, & Eisenberg, 2004; Janowski et al., 2001; Knaus et al., 2001). HCC is the first disease-causing amyloidogenic protein whose oligomerization has been shown to occur via a 3D domain swapping process, with the L68Q variant showing a greater propensity for this process (Sanders et al., 2004; Staniforth et al., 2001). Previously, using molecular dynamics (MD) simulation, our group demonstrated that the hydrophobic core region of cC I66Q mutant was expanded compared with WT cC and AS had larger displacements in the I66Q mutant, these structural difference persisted throughout the whole time course of the simulation (Yu et al., 2012). These findings suggested that the AS in amyloidogenic cystatin may play an important role in opening the native structure and triggering the process of domain swapping.

Recently, disulfide bond and salt bridge formation have been identified as specific interactions that can stabilize aggregation–prone interfaces in native protein conformations and thus prevent structural rearrangements that are required for misfolding and aggregation (Pechmann, Levy, Tartaglia, & Vendruscolo, 2009). A previous study by Björk and Ylinenjarvi showed that the Cys95–Cys115 disulfide bond, but not the Cys71–Cys81 bond of cC, is of more importance for maintaining the native conformation of cC and is crucial for its proteinase-binding ability (Björk & Ylinenjarvi, 1992). The formation of disulfide bonds has been associated with stabilizing interaction between protein secondary structures, for example, disulfide bonds that close long loops are reportedly more efficient for stabilizing proteins than those closing short loops (Abkevich & Shakhnovich, 2000). In addition to loops (Schirra, Guarino, Anderson, & Craik, 2010), disulfide bridges are also known to stabilize β-sheets (Venkatraman, Nagana Gowda, & Balaram, 2002) and α-helices (Kibria & Lees, 2008) in the correct conformations of proteins. However, their effect on turn structures (e.g. β-turn or hairpins) depends on the amino acid content of the turn (Santiveri, Leon, Rico, & Jimenez, 2008). Taken together, this led us to hypothesize that the formation of either one, or both, of the two native disulfide bonds of cC may be a critical factor for sustaining and stabilizing the native structure; and conversely, breakage of either one, or both, might be influential in the process of domain swapping and hence amyloid formation.

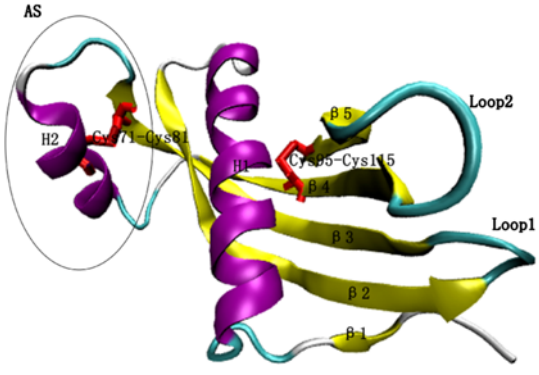

Figure 1. Structural representation of chicken cystatin, the two disulfide bridges are displayed by red sticks, colored magenta, yellow, and cyan are the α–helix, the β-strand, and the loops, respectively.

In this study, we have used a combination of biochemical and computational approaches to investigate the influence of the Cys71–Cys81 and Cys95–Cys115 disulfide bonds on stability of cC I66Q mutant. Our results demonstrate the significance of both disulfide bonds in the formation of cC I66Q mutant native structure and provide further insight into key determinants that influence domain swapping in cC and hence amyloid formation.

Materials and methods

Expression and purification of recombinant cCs

pPICZαA expression vectors encoding both WT and I66Q mutant cC proteins were introduced into *Pichia pastoris*, and protein was expressed and purified as described previously (He et al., 2005). However, the ammonium precipitation approach was not performed, following cell lysis and the insoluble protein aggregates were removed by centrifugation, the supernatants were diluted one in five and applied on a CM-Toyopearl column. The absorbed recombinant cC proteins were eluted using a gradient of 0–.5 M sodium chloride in 20 mM Tris–HCl buffer, pH 7.5 and fractions collected. The protein content of each fraction was determined by measuring the absorbance at 280 nm as well as sodium dodecyl sulfate polyacrylamide gel electrophoresis (SDS-PAGE). The fraction containing the protein was collected and dialyzed against deionized water to remove salt at 4 °C.

Tricine–SDS-PAGE

The Tricine–SDS-PAGE was run under nonreducing conditions. The protein samples were fractionated by

Tricine–SDS-PAGE as described by Schägger (2006). The sample (30 μL) was pretreated by mixing with 10 μL 4 × SDS-PAGE loading buffer (Buffer B: 12% SDS (wt/vol), 30% glycerol (wt/vol), .05% coomassie blue G-250 (Serva), 150 mM Tris/HCl (pH 7.0) in a .5 mL centrifugal tube). To examine disulfide bond status, dithiothreitol (DTT) was added at different concentrations: 0, 1, 2, and 4 mM. After mild shaking for 5 s, the samples were incubated at 37 °C for 10 min, then each sample aliquot (10 μL) was loaded to the sample wells. Electrophoresis of the protein was performed on 16% separating gel containing glycerol and 4% stacking gel. The gels were kept at a constant voltage of 60 and 120 V at stacking and resolving gel, respectively. Protein staining was carried out using coomassie brilliant blue.

Circular dichroism analysis

Far-ultraviolet (200–260 nm) circular dichroism (far-UV CD) spectra were measured to estimate the conformational change in recombinant cystatins according to the method of Kato and Tanimoto (Kato, Tanimoto, Muraki, Kobayashi, & Kumagai, 1992). Recombinant cystatin solutions were adjusted to .05 mg/mL with 10 mM phosphate buffer (pH 7.0). CD spectra were recorded at 25 °C on a J-600 spectropolarimeter (Jasco, Tokyo, Japan) with a 1.0 cm cuvette.

Construction of different I66Q mutant cC monomer models

The model of the monomeric molecule used in our work is based on the X-ray crystal structure of the coordinates of monomeric chicken cystatin (protein data bank [PDB] entry 1CEW), which was obtained from research collaboratory for structural bioinformatics Protein Data Bank (Bode et al., 1988). The model of I66Q monomer was constructed using homologous modeling method through the online service of Swiss Model (http://swissmodel.expasy.org/). In this study, the same PDB file of WT and I66Q mutant cC was used to construct different initial conformations for simulations: the native state (referred to as NAT), the disulfide bond between Cys71–Cys81 reduced state (this disulfide bond broken state is abbreviated as DBBS C71-C81), Cys95–Cys115 reduced state (DBBS C95-C115), and both disulfide bonds reduced state (DBBS BOTH).

MD simulations

All MD simulations were carried out by GROMACS 4.0.7 software package (Hess, Kutzner, Van Der Spoel, & Lindahl, 2008) with constant number, pressure, temperature, and periodic boundary conditions. The V-rescale and Parrinello–Rahman algorithms have been applied for temperature and pressure coupling, respectively. The GROMOS96 43a1 (Scott et al., 1998) force field was applied in all simulations. The models were immersed in the cubic boxes filled with water molecules with a distance between peptides and box edges of at least 10 Å. Each monomer model was solvent in a water box approximately containing 10,124 simple point-charge water molecules (Berendsen, Postma, van Gunsteren, & Hermans, 1981) and neutralized by adding 14 Cl^- counter ions. The linear constraint solver method (Berendsen et al., 1981) was used to constrain bond lengths, allowing an integration step of 2 fs. Electrostatic interactions were calculated with the particle mesh Ewald algorithm (Essmann et al., 1995). All calculations were carried out with a cutoff of 9 Å. The solvated and neutralized systems were then energy-minimized for 20 ps to remove bad contacts. Afterwards, the backbone atoms of the structure were fixed, while the side chains and solvent were allowed to move unrestrained for 40 ps. After equilibration, the total of four independent simulations was carried out at 330 K, pH2 for 20 ns, respectively.

Analytic methods

The GROMACS package was used for most analyses performed. Secondary structure analyses were carried out employing the defined secondary structure of protein (DSSP) method (Kabsch & Sander, 1983). The Visual Molecular Dynamics software (VMD) was used to produce all images. The root-mean-square deviations (RMSD) were calculated for all alpha– carbon (C) atoms with reference to the first frame of the trajectories. H–bonds were calculated by a distance cutoff of 3 Å and an angle cutoff of 120°.

Results

Different disulfide bond status exists between WT cC and I66Q mutant

Staniforth et al. demonstrated that in contrast to WT cC, which had an immeasurably slow dimerization rate, the I66Q cC mutant dimerizes spontaneously and rapidly at room temperature in the absence of denaturant (Staniforth et al., 2001). Therefore, in order to investigate the role that the disulfide bond formation may play in dimerization, we decided to assess the disulfide bond states of I66Q compared to WT under conditions that I66Q spontaneously dimerizes.

Generally, Laemmli SDS-PAGE was primarily used for separating proteins >30 kDa, while Tricine–SDS-PAGE was used preferentially for the optimal separation of proteins <30 kDa. Thus, to detect the different disulfide bond forms in the two cC proteins, we developed a protein laddering map using Tricine–SDS-PAGE, which is mainly based on a similar method using SDS-PAGE (Wu et al., 2010). Compared with reducing SDS-PAGE under extensively reducing conditions, the electrophoretic mobility of proteins containing incomplete disulfide bonds on nonreducing SDS-PAGE has a minute

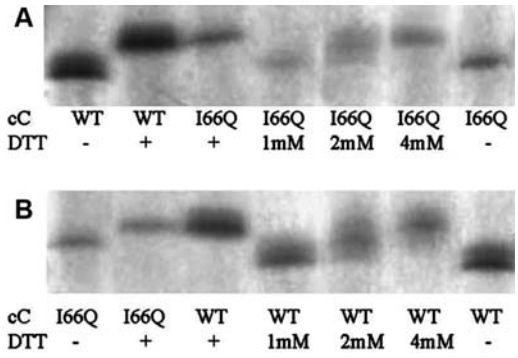

Figure 2. I66Q mutant exhibits different disulfide bond variants under physiological conditions compared with WT cC. A, B Tricine–SDS-PAGE patterns of WT and I66Q cC mutant following incubation with or without different concentrations of DTT. After incubation, the samples were subjected to nonreducing Tricine–SDS-PAGE. '+' represents reaction of cC with 8 mM DTT, this concentration of DTT is sufficient to maintain both disulfide bonds in the reduced state, while '–' represents no DTT treatment.

difference due to different compact conformations of proteins with disulfide bonds. Using Tricine–SDS-PAGE which enables a better resolution compared to SDS-PAGE, such structural differences are clearly visible. Figure 2 shows that WT cC exhibits three disulfide bond variants: these being the protein with two disulfide bonds, one disulfide bond, and no disulfide bonds (following reduction by DTT), respectively. In contrast, after reduction with DTT or nonreducing sample buffer followed by incubation at 37 °C for 10 min, the I66Q mutant showed only two disulfide bond variants: these containing one disulfide bond and no disulfide bond, respectively. This suggests that one of the two disulfide bonds that exists in WT cC has been disrupted during or before the process of dimerization, in the I66Q mutant.

Dynamics of cC structural changes

It has been proved that in MD simulations, high temperature and low pH value can accelerate protein unfolding without changing the pathway of unfolding (Day, Bennion, Ham, & Daggett, 2002). Therefore, we performed the simulations under the extreme conditions with the elevated temperature of 330 K (57 °C) and pH2, to correspond with the conditions that were chosen in our previous experiments (He et al., 2005; Yu et al., 2010, 2012) and further make the system reach the equilibrated regions at a minimum of simulation time and computational expense. The RMSDs of the backbone alpha carbon atoms of cC during molecular dynamic simulations were calculated for all simulations. The RMSD value reached a relative equilibrium region at 10 ns in both I66Q and WT cC (Figure 3(A)), and energy analysis showed all system reached convergence (data not shown).

In two WT simulations (native and both disulfide bonds reduced) and the I66Q native simulation, the RMSDs are similar at around .25 nm during the 20 ns simulations. However, the residue averages of the root-mean-square fluctuations (RMSF) values and secondary structure contents during the 20 ns MD simulations show that the untwisting of the Helix 2 of WT DBBS BOTH, I66Q NAT are more apparent compared to WT NAT and the Helix 1 content of I66Q NAT is slightly reduced (data not shown). Owing to that change in the content of Helix's 1 and 2 has an obvious influence on cystatin amyloidogenic properties (He et al., 2005; Yu et al., 2010, 2012), these results suggested that the three systems may exist some differences in aggregation capabilities although three RMSDs are similar. In contrast, other conformations of I66Q series with different disulfide bond variants showed higher RMSDs than both WT simulations and the I66Q native simulation. Interestingly,

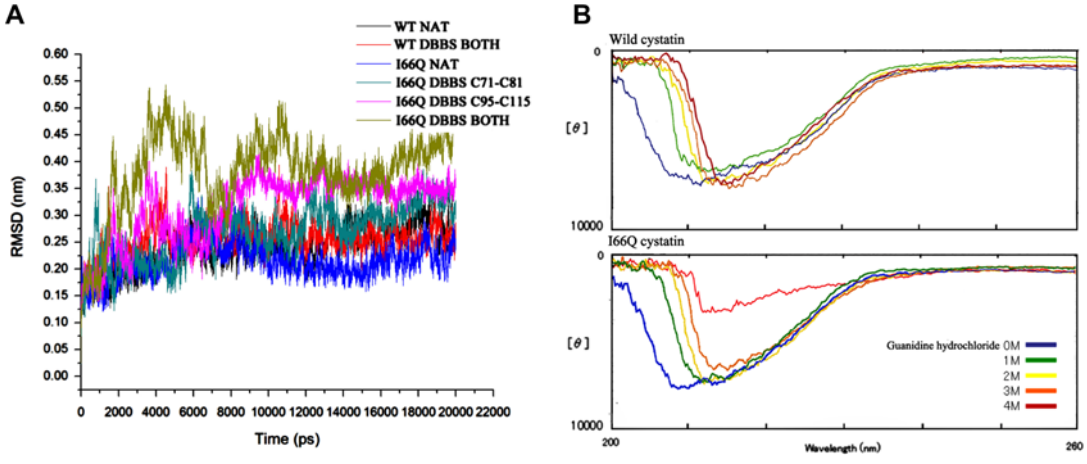

Figure 3. (A) RMSDs of the Cα-positions during the 20 ns simulations. (B) Far-UV CD spectra for WT and I66Q mutant in native state and in presence of increasing amounts of denaturant.

the RMSD of Cys95–Cys115 reduced form (I66Q DBBS C95-C115) is broadly comparable with the simulation in which both disulfide bonds are reduced (I66Q DBBS BOTH), but is higher than the simulation for the Cys71–Cys81 reduced form (I66Q DBBS C71-C81). The results of I66Q DBBS C71–C81 and I66Q DBBS C95–C115 are consistent with a previous study in which it was suggested that the less accessible Cys95–Cys115 disulfide bond of cC, (compared to the more accessible Cys7l–Cys81 bond), is of greater importance for maintaining the conformation of the inhibitor required for binding of target proteinases (Bjork & Ylinenjarvi, 1992).

In addition, this result also suggests that the conformational stability of I66Q is more responsive and sensitive to changes in disulfide bond status compared to WT cC. Thus, MD simulations predict a much-increased fluctuation in structural conformations for the Cys95–Cys115 reduced I66Q mutant. These structural changes could be much more pronounced in a multimolecular system, and hence could possibly aid in inducing domain swapping between I66Q mutant molecules.

I66Q cC mutant showed significant structural changes under denaturing conditions comparing with WT cC

To assess if conformational stability of I66Q is indeed more sensitive to disulfide bond status compared with WT cC, far-UV CD spectra were recorded for both WT and I66Q cC mutant in native and increasingly denaturing conditions (in presence of 1–4 M GdmCl) (Figure 3 (B)). The unfolding profile of WT cC and I66Q cC mutant was assessed at 37 °C with different GdmCl concentrations for 30 min period using far-UV CD spectroscopy. Up to a concentration of 3 M GdmCl, both WT and I66Q cC display a very similar denaturation profile (Figure 3(B)). However, upon further reducing power of 4 M GdmCl, a significant change in the secondary structure was observed for I66Q, which is in stark contrast to WT cC which was not perturbed under these experimental conditions. These results suggest that the disruption of disulfide bonds in the I66Q mutant greatly affects the conformational stability of the compact structure of the cC monomer, much more readily than the equivalent WT cC monomer.

Analysis of the distance between sulfur atoms in cysteine residues of I66Q mutant within various disulfide bond variants

Previous studies have shown that domain swapping of stefins (cystatin superfamily I) and Hcc requires that almost the complete unfolding of native structure before the two chains can rearrange and swap strands (Jerala & Zerovnik, 1999; Zerovnik et al., 2011). Hence, to further assess importance of sequence of disulfide bond breakage in the unfolding process of I66Q cC mutant, we analyzed the distance between sulfur atoms in cysteine

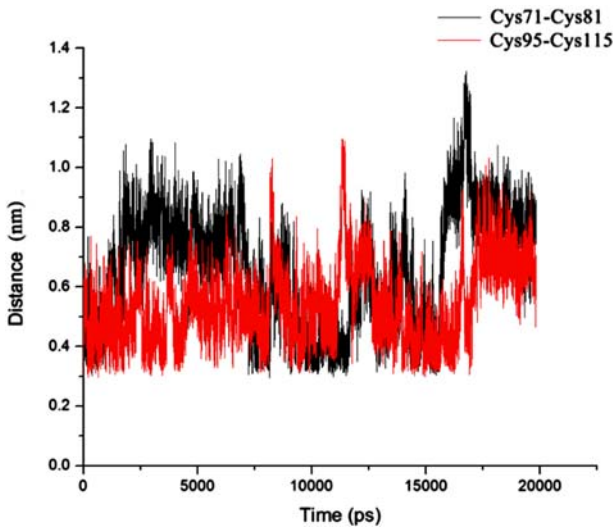

Figure 4. Distance between sulfur atoms in cysteine residues of I66Q DBBS BOTH.

residues started with the disulfide bond completely reduced form (i.e. disulfide bond nonprotected form, I66Q DBBS BOTH) during MD simulations (Figure 4). Our data show that early in the simulation there is a major structural change in the I66Q mutant that causes a significant increase in distance (> .8 nm at 2 ns) between Cys71 and Cys81, while Cys95 and Cys115 distance remains reasonably constant. Subsequently, later in the simulation, the Cys95–Cys115 region begins to change which may be a crucial factor in causing loss of enzymatic activity. This is corresponding with our previous experimental finding, i.e. both the I66Q and WT cCs have similar inhibitory activity toward papain (He et al., 2005). Taken together, it suggests that at 37 °C the Cys71–Cys81 disulfide bond might be disrupted in the I66Q, while the Cys95–Cys115 disulfide bond might be preserved in these conditions. We predict that the inherent structural differences between the WT cC and the I66Q mutant increases the probability of disruption of the Cys71–Cys81 disulfide bridge and hence increases the accessibility of the monomeric I66Q structure.

Residue averages of the RMSF in various I66Q simulations

To assess the detailed structural changes occurring in the monomeric I66Q mutant with respect to different states of disulfide bond breakage, we calculated the average RMSF during the convergence period of MD simulations (10–20 ns) of Cα for each residue of the protein (Figure 5 (A)). The RMSF results showed that the AS region (consisting of Helix 2) has a comparatively large displacement in all models, although this is much more pronounced following disruption of the disulfide bridges. Helix 2 partially unfolded to β-turns in each model lacking disulfide bonds, but it maintains a helical structure in

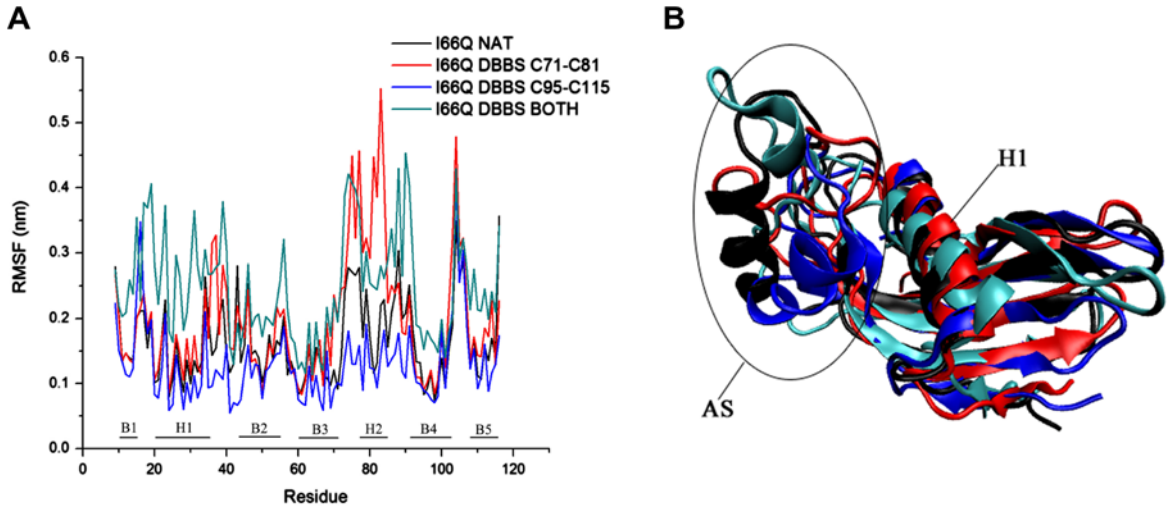

Figure 5. (A) Averaged Cα RMSFs per residue in water during the convergence period of MD simulations. The secondary structure elements are also shown. (B) Superposition of various states of I66Q mutant structures at the end of the 20 ns MD simulation.

the native state model (Figure 5(B)). This data suggests that the unfolding of Helix 2 is a major factor in the large displacement of AS region in the I66Q mutant. Of particular significance is that the Helix 1 region, which is included in the α–β interface, also has very obvious structural fluctuations in the completely reduced state (I66Q DBBS BOTH) compared with the native state or single disulfide bond disrupted models (Figure 5(A) and (B)). This implies that the α–β interface may play an important role in induction of domain swapping, and at the very least that unfolding of the AS region may not be the only structural factor influencing this process.

In order to assess the dynamic characteristics of the structural changes in various states of the I66Q mutant models, we used the DSSP algorithm to analyze the α-helix and β-sheet content during the whole time frame of the MD simulations (Figure 6(A) and (B)). The α-helix content of various I66Q reduced disulfide states significantly decreased throughout the MD simulation, which is in contrast to the native state (Figure 6(A)). This difference is primarily caused by the unfolding of Helix 2 in the AS region. Since the Cys71–Cys81 disulfide bridge is located in the AS region, it is reasonable to presume that the breakage of Cys71–Cys81 induced the unfolding of Helix 2. Intriguingly, the α-helix content in the Cys95–Cys115 reduced state decreased dramatically to 17% (18 residues), which is similar to the Cys71–Cys81 disulfide bond reduced system. It suggests that the Cys71–Cys81 disulfide bond reduction is a prerequisite for displacement of the AS region and unfolding of Helix 2. In general, the β-sheet content fluctuated dramatically during the whole 20 ns simulations, for all I66Q models (Figure 6(B)). In the native state, the β-sheet content initially decreases, but stabilizes at 43% finally, similar to the other states by the end of the simulation. These large and frequent perturbations suggested that the β-sheet structures were extremely unstable in these extreme conditions (pH2.0, 330 K). However, due to the restriction of simulation time scale, the β-sheet content did not show significant change when assessed at the simulation start and finish points.

Analysis of the α–β interface distance of various I66Q mutant

Although the secondary structure analysis showed that Helix 1 content did not change (data not shown), Helix 1 displayed a relatively large displacement during the simulation (Figure 5(A)). We therefore analyzed the α–β interface distance (the α–β interface distance was defined as the distance between the mass center of α-helix and mass center of β3–β4 strands), a factor already shown to be important in domain swapping in the HCC L68Q mutant (Rodziewicz-Motowidlo et al., 2006). We found that each I66Q with reduced disulfide bonds exhibited a larger distance between α and β interface compared to the native I66Q mutant (Figure 7). The average distances during the final 10 ns of the simulation were .731, .805, .812, and .895 nm for native state, Cys71–Cys81 reduced state, Cys95–Cys115 reduced state, and both reduced state, respectively. The diagram clearly shows that Helix 1 of different disulfide bond reduced states has moved away from the β-sheet interface, compared to the native state. The calculations for hydrogen bond formation between the α and β interface indicate a reduced number of hydrogen bonds in the double disulfide bond reduced states (data not shown). The larger α–β interface distance displays a larger solvent accessible surface than that of the native mutant and the increased flexibility of the exchangeable fragment could explain the higher tendency for dimer formation of the I66Q mutant.

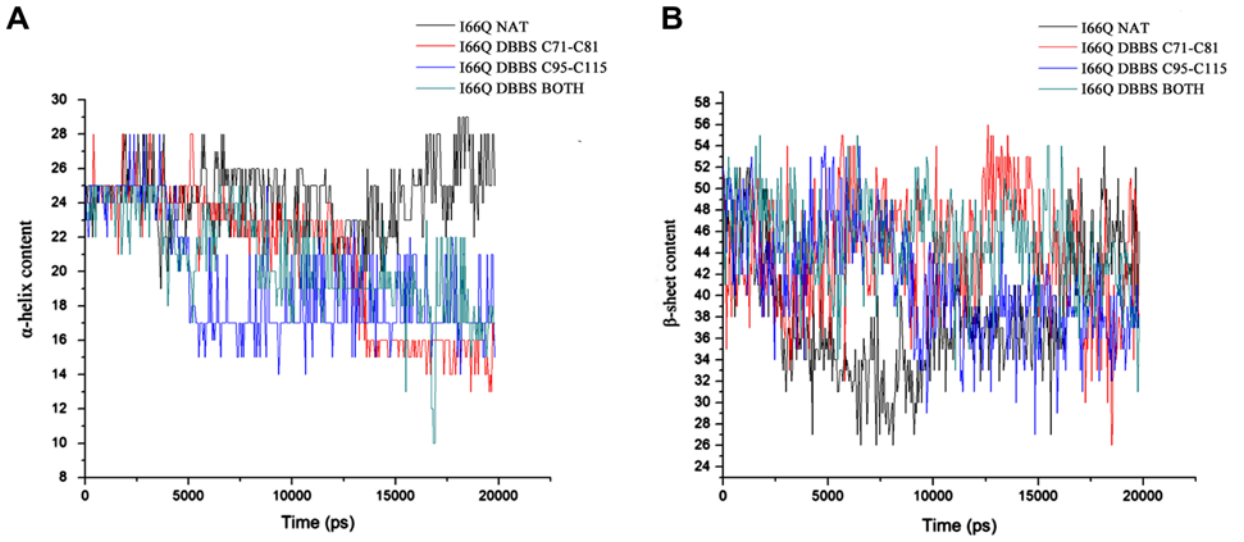

Figure 6. The content of α-helix (A) and β-sheet (B) in various I66Q mutants as a function of simulation time.

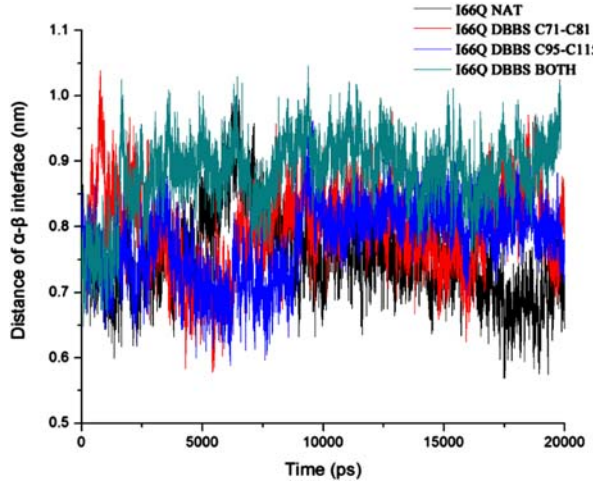

Figure 7. The α–β interface distance as a function of simulation time.

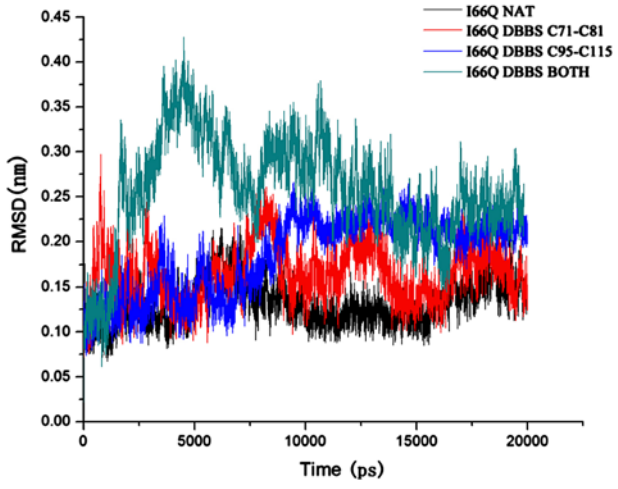

Figure 8. RMSDs of the hydrophobic core backbone during the 20 ns simulations.

The structural stability of the hydrophobic core results in various I66Q states

The interior hydrophobic core of cystatin provides the structural stability that favors the native state during the protein folding process (Bode et al., 1988; Zhao et al., 2009). In a previous study from our group, we demonstrated that mutation of residues within hydrophobic core induced expansion of the core and exposed an array of inner hydrophobic residues to solvent environment (Yu et al., 2010). This would most likely destabilize the molecular α–β interface and may induce or influence domain swapping. We therefore analyzed the effects of disulfide bridge disruption on the structure of the cC hydrophobic core by calculating the RMSD for hydrophobic core residues during the 20 ns simulations. Figure 8 shows that I66Q DSSB BOTH model is the most unstable across the whole time frame of the simulation. During the final 10 ns of the simulation, the I66Q DBBS C95–C115 model has a very similar profile as the I66Q DSSB BOTH model. The RMSD of I66Q DBBS C71-C81 slightly exceeded that of I66Q native state at various time points along the simulation, but at 20 ns reached a similar value to the native form. The I66Q DBBS BOTH and I66Q DBBS C95–C115 models maintain the largest RMSDs value by the end of the simulations, indicating the hydrophobic core of these reduced states was more flexible than the I66Q DBBS C71-C81 or the native state. This result suggests that disruption of the Cys95–Cys115 disulfide bond is more influential in inducing hydrophobic core expansion compared with the

Cys71–Cys81 disulfide bond. This finding matches well with the structural data and conclusions presented in Figures 3 and 4.

Discussion

The incomplete folding of some proteins leads to their deposition in the form of amyloid fibrils, a state that is the origin of a variety of human diseases (Grana-Montes et al., 2012). The formation of disulfide bonds influences the protein folding process and can impact on the formation of amyloid fibrils (Grana-Montes et al., 2012). The I66Q mutation in the hydrophobic core of cC protein destabilizes the native conformation and is associated with pathological phenotypes similar to HCC protein. Adapting Tricine–SDS-PAGE analysis, we demonstrate for the first time that under the physiological conditions, the I66Q mutant of cC is deficient in disulfide bond formation compared to native cC. Our data suggest that I66Q dimerization is much more likely to occur spontaneously compared to the native form. Taken together the CD results and RMSDs of protein, Cα-positions suggest that the conformational stability of I66Q is much more sensitive and responsive to changes in disulfide bond status compared to WT cC, indicating that the breakage of disulfide bonds facilitates conversion of I66Q to an unfolded form with a propensity for amyloid formation. Accordingly, disulfide bond reduction in the I66Q mutant may act as key molecular determinant of protein unfolding and a pivotal triggering factor for domain swapping and dimerization, in the context of fibrillation.

As Bjork and Ylinenjarvi previously reported, the short-range Cys95–Cys115 disulfide bond was considered to be more important in stabilizing global folding of the WT cC, rather than the Cys71–Cys81 disulfide bond (Bjork & Ylinenjarvi, 1992). When assessing the molecular distances between the disulfide forming residues in the fully reduced I66Q model, we found that larger perturbations were found in the Cys71–Cys81 region of the protein (Figure 4). Similarly, our recent study assessing the role of the AS structure in dimerization of cystatin prior to domain swapping, also demonstrated that the disulfide bond within the AS (Cys71–Cys81) in cC I66Q was dramatically perturbed from 10 ns in the simulation; while in WT cC, this region was relatively stable (Yu et al., 2012). Overall, the data suggest that the AS domain and disulfide bridge Cys71–Cys81 have a higher propensity for structural perturbation than the region of the protein harboring the Cys95–Cys115 disulfide bond. Furthermore, the breakage of the Cys71–Cys81 disulfide bond has a high impact on the I66Q mutant's unfolding process and may play a major role in triggering domain swapping and dimerization. Further analysis of the structural change in various reduced states of the I66Q mutant confirmed that the decrease α-helical content is mainly due to the unfolding of Helix 2 in the AS region. Although the breakage of Cys95–Cys115 disulfide bond also resulted in a similar decrease of α-helical content, the breakage of the much more highly accessible Cys71–Cys81 disulfide bond would have a greater impact on protein unfolding due to disruption of Helix 2 and therefore displacement of the AS region.

It has been proposed that in the case of L68Q variant of HCC, this mutation most likely destabilizes the α–β molecular interface through repulsive forces on the α-helix due to the larger and chemically incompatible side chain at position 68, thus inducing the molecule to unfold into the α- and β-subdomains (Janowski et al., 2001). Our observations support this proposal since the breakage of either of the two disulfide bonds in I66Q causes a dramatic increase in the α–β interface distance. The larger RMSDs value at the end of the simulations for I66Q DBBS BOTH and I66Q DBBS C95-C115 variants illustrated that the hydrophobic core in these variants was more flexible than the other variants, indicating that the Cys95–Cys115 disulfide bond is of more significance in inducing hydrophobic core expansions compared with the Cys71–Cys81 disulfide bond. Our previous data measuring enzyme activity of the I66Q monomer suggested that the I66Q mutant maintained the conformation required for inhibition and binding of target proteinases and lead us to speculate that the Cys95–Cys115 disulfide bond of I66Q is preserved in the monomeric state (He et al., 2006). An additional research issue to be tackled is whether there are big/subtle differences in each building blocks' secondary structure of the I66Q mutant and its disulfide bridge reduction variants, further *in silico* studies on some geometrical properties, such as the number of hydrogen bonds, the number of native contacts, the solvent accessible surface area, and Rg values would provide an explicit interpretation.

Our observations are also in accordance with the study of Kolodziejczyk et al. (2010), in which they found that ionizing radiation-driven disruption of a disulfide bonds in HCC resulted in breakage of the Cys73–Cys83 disulfide bridge (corresponding to Cys71–Cys81 bridge in cC) of HCC molecule A (molecule A and B are the two monomers en route to dimerization). In contrast, the second native disulfide bond, Cys97–Cys117 (corresponding to Cys95–Cys115 bridge in cC), remained intact in both molecules (Kolodziejczyk et al. 2010).

In summary, we have demonstrated experimentally that the I66Q mutant of cC is altered in terms of the number of disulfide bridges present in the structure, compared to native cC. *In silico* studies suggest that this difference may represent a key factor in determining the molecular level propensity of the I66Q mutant to undergo domain swapping and formation of amyloid fibrils. Further experimental and computational studies on the relationship between disulfide bond formations with a variety of cC

mutants will provide valuable insight and help elucidate the possible direct and indirect influence of disulfide bond status on domain swapping, dimerization, and amyloid fibril formation of the cystatins.

Acknowledgment

This work was supported by grants from National Natural Science Foundation of China (No. 30970152) and partially sponsored by the Fund of Liaoning Provincial Education Department (No. 2009R26). The Project was also sponsored by the Scientific Research Foundation for the Returned Overseas Chinese Scholars, State Education Ministry (No. [2010]1561).

Abbreviations

cC	–	Chicken cystatin
HCC	–	Human cystatin C
AS	–	Appendant structure
RMSD	–	Root-mean-square deviation
VMD	–	Visual molecular dynamics
DBBS	–	Disulfide bond broken state
H-bond	–	Hydrogen bond

Reference

Abkevich, V.I., & Shakhnovich, E.I. (2000). What can disulfide bonds tell us about protein energetics, function and folding: Simulations and bioinformatics analysis. *Journal of Molecular Biology, 300*, 975–985.

Abrahamson, M. (1996). Molecular basis for amyloidosis related to hereditary brain hemorrhage. *Scandinavian Journal of Clinical and Laboratory Investigation, 226*(Supplement), 47–56.

Berendsen, H.J.C., Postma, J.P.M., van Gunsteren, W.F., & Hermans, J. (1981). Interaction models for water in relation to protein hydration. *Intermolecular forces, 11*(supplement 1), 331–338.

Bjork, I., & Ylinenjarvi, K. (1992). Different roles of the two disulfide bonds of the cysteine proteinase inhibitor, chicken cystatin, for the conformation of the active protein. *Biochemistry, 31*, 8597–8602.

Bobek, L.A., & Levine, M.J. (1992). Cystatins-inhibitors of cysteine proteinases. *Critical Reviews in Oral Biology and Medicine, 3*, 307–332.

Bode, W., Engh, R., Musil, D., Thiele, U., Huber, R., Karshikov, A., … Turk, V. (1988). The 2.0 A X-ray crystal structure of chicken egg white cystatin and its possible mode of interaction with cysteine proteinases. *EMBO Journal, 7*, 2593–2599.

Day, R., Bennion, B.J., Ham, S., & Daggett, V. (2002). Increasing temperature accelerates protein unfolding without changing the pathway of unfolding. *Journal of Molecular Biology, 322*, 189–203.

Ekiel, I., Abrahamson, M., Fulton, D.B., Lindahl, P., Storer, A.C., Levadoux, W., … Gehring, K. (1997). NMR structural studies of Human Cystatin C dimers and monomers. *Journal of Molecular Biology, 271*, 266–277.

Engh, R.A., Dieckmann, T., Bode, W., Auerswald, E.A., Turk, V., Huber, R., & Oschkinat, H. (1993). Conformational variability of chicken cystatin. Comparison of structures determined by X-ray diffraction and NMR spectroscopy. *Journal of Molecular Biology, 234*, 1060–1069.

Essmann, U., Perera, L., Berkowitz, M.L., Darden, T., Lee, H.J., & Pedersen, L.G. (1995). A smooth particle mesh Ewald potential. *Journal of Chemical Physics, 103*, 8577–8592.

Grana-Montes, R., de Groot, N.S., Castillo, V., Sancho, J., Velazquez-Campoy, A., & Ventura, S. (2012). Contribution of disulfide bonds to stability, folding, and amyloid fibril formation: The PI3-SH3 domain case. *Antioxidants & Redox Signaling, 16*, 1–15.

Grubb, A., Jensson, O., Gudmundsson, G., Arnason, A., Lofberg, H., & Malm, J. (1984). Abnormal metabolism of gamma-trace alkaline microprotein. The basic defect in hereditary cerebral hemorrhage with amyloidosis. *New England Journal of Medicine, 311*, 1547–1549.

He, J., Song, Y., Ueyama, N., Harada, A., Azakami, H., & Kato, A. (2005). Characterization of recombinant amyloidogenic chicken cystatin mutant I66Q expressed in yeast. *Journal of Biochemistry, 137*, 477–485.

He, J., Song, Y., Ueyama, N., Saito, A., Azakami, H., & Kato, A. (2006). Prevention of amyloid fibril formation of amyloidogenic chicken cystatin by site-specific glycosylation in yeast. *Protein Science, 15*, 213–222.

Hess, B., Kutzner, C., Van Der Spoel, D., & Lindahl, E. (2008). GROMACS 4: Algorithms for highly efficient, load-balanced, and scalable molecular simulation. *Journal of Chemical Theory and Computation, 4*, 435–447.

Ivanova, M.I., Sawaya, M.R., Gingery, M., Attinger, A., & Eisenberg, D. (2004). An amyloid-forming segment of beta2-microglobulin suggests a molecular model for the fibril. *Proceedings of National Academy Sciences USA, 101*, 10584–10589.

Janowski, R., Kozak, M., Jankowska, E., Grzonka, Z., Grubb, A., Abrahamson, M., & Jaskolski, M. (2001). Human cystatin C, an amyloidogenic protein, dimerizes through three-dimensional domain swapping. *Natural Structural Biology, 8*, 316–320.

Jerala, R., & Zerovnik, E. (1999). Accessing the global minimum conformation of stefin a dimer by annealing under partially denaturing conditions. *Journal of Molecular Biology, 291*, 1079–1089.

Kabsch, W., & Sander, C. (1983). Dictionary of protein secondary structure: Pattern recognition of hydrogen-bonded and geometrical features. *Biopolymers, 22*, 2577–2637.

Kaeser, S.A., Herzig, M.C., Coomaraswamy, J., Kilger, E., Selenica, M.L., Winkler, D.T., … Jucker, M. (2007). Cystatin C modulates cerebral beta-amyloidosis. *Nature Genetics, 39*, 1437–1439.

Kato, A., Tanimoto, S., Muraki, Y., Kobayashi, K., & Kumagai, I. (1992). Structural and functional properties of hen egg-white lysozyme deamidated by protein engineering. *Bioscience, Biotechnology, and Biochemistry, 56*, 1424–1428.

Kibria, F.M., & Lees, W.J. (2008). Balancing conformational and oxidative kinetic traps during the folding of bovine pancreatic trypsin inhibitor (BPTI) with glutathione and glutathione disulfide. *Journal of the American Chemical Society, 130*, 796–797.

Knaus, K.J., Morillas, M., Swietnicki, W., Malone, M., Surewicz, W.K., & Yee, V.C. (2001). Crystal structure of the human prion protein reveals a mechanism for oligomerization. *Natural Structural Biology, 8*, 770–774.

Kolodziejczyk, R., Michalska, K., Hernandez-Santoyo, A., Wahlbom, M., Grubb, A., & Jaskolski, M. (2010). Crystal structure of Human Cystatin C stabilized against amyloid formation. *FEBS Journal, 277*, 1726–1737.

Mi, W., Pawlik, M., Sastre, M., Jung, S.S., Radvinsky, D.S., Klein, A.M., … Levy, E. (2007). Cystatin C inhibits amyloid-beta deposition in Alzheimer's disease mouse models. *Nature Genetics, 39*, 1440–1442.

Olafsson, I., & Grubb, A. (2000). Hereditary cystatin C amyloid angiopathy. *Amyloid, 7*, 70–79.

Pechmann, S., Levy, E.D., Tartaglia, G.G., & Vendruscolo, M. (2009). Physicochemical principles that regulate the competition between functional and dysfunctional association of proteins. *Proceedings of National Academy of Sciences USA, 106*, 10159–10164.

Rodziewicz-Motowidlo, S., Wahlbom, M., Wang, X., Lagiewka, J., Janowski, R., Jaskolski, M., … Grzonka, Z. (2006). Checking the conformational stability of cystatin C and its L68Q variant by molecular dynamics studies: Why is the L68Q variant amyloidogenic? *Journal of Structural Biology, 154*, 68–78.

Sanders, A., Jeremy Craven, C., Higgins, L.D., Giannini, S., Conroy, M.J., Hounslow, A.M., … Staniforth, R.A. (2004). Cystatin forms a tetramer through structural rearrangement of domain-swapped dimers prior to amyloidogenesis. *Journal of Molecular Biology, 336*, 165–178.

Santiveri, C.M., Leon, E., Rico, M., & Jimenez, M.A. (2008). Context-dependence of the contribution of disulfide bonds to beta-hairpin stability. *Chemistry, 14*, 488–499.

Schagger, H. (2006). Tricine–SDS-PAGE. *Nature Protocols, 1*, 16–22.

Schirra, H.J., Guarino, R.F., Anderson, M.A., & Craik, D.J. (2010). Selective removal of individual disulfide bonds within a potato type II serine proteinase inhibitor from *Nicotiana alata* reveals differential stabilization of the reactive-site loop. *Journal of Molecular Biology, 395*, 609–626.

Scott, W.R.P., Hünenberger, P.H., Tironi, I.G., Mark, A.E., Billeter, S.R., Fennen, J., … van Gunsteren, W.F. (1998). The GROMOS biomolecular simulation program package. *Journal of Physical Chemistry A, 103*, 3596–3407.

Staniforth, R.A., Giannini, S., Higgins, L.D., Conroy, M.J., Hounslow, A.M., Jerala, R., … Waltho, J.P. (2001). Three-dimensional domain swapping in the folded and molten-globule states of cystatins, an amyloid-forming structural superfamily. *EMBO Journal, 20*, 4774–4781.

Venkatraman, J., Nagana Gowda, G.A., & Balaram, P. (2002). Design and construction of an open multistranded beta-sheet polypeptide stabilized by a disulfide bridge. *Journal of the American Chemical Society, 124*, 4987–4994.

Wu, D., Ma, D., Hao, Y.Y., Chu, J., Wang, Y.H., Zhuang, Y.P., & Zhang, S.L. (2010). Incomplete formation of intramolecular disulfide bond triggers degradation and aggregation of human consensus interferon-alpha mutant by *Pichia pastoris*. *Applied Microbiology and Biotechnology, 85*, 1759–1767.

Yu, Y., Liu, X., He, J., Zhang, M., Li, H., Wei, D., & Song, Y. (2012). Appendant structure plays an important role in amyloidogenic cystatin dimerization prior to domain swapping. *Journal of Biomolecular Structure & Dynamics, 30*, 102–112.

Yu, Y., Wang, Y., He, J., Liu, Y., Li, H., Zhang, H., & Song, Y. (2010). Structural and dynamic properties of a new amyloidogenic chicken cystatin mutant I108T. *Journal of Biomolecular Structure & Dynamics, 27*, 641–649.

Zerovnik, E., Stoka, V., Mirtic, A., Guncar, G., Grdadolnik, J., Staniforth, R.A., … Turk, V. (2011). Mechanisms of amyloid fibril formation–focus on domain-swapping. *FEBS Journal, 278*, 2263–2282.

Zhao, J.H., Liu, H.L., Liu, Y.F., Lin, H.Y., Fang, H.W., Ho, Y., & Tsai, W.B. (2009). Molecular dynamics simulations to investigate the aggregation behaviors of the Abeta(17–42) oligomers. *Journal of Biomolecular Structure & Dynamics, 26*, 481–490.